EECoG-Comp: An Open Source Platform for Concurrent EEG/ECoG Comparisons

Qing Wang[1] · Pedro Antonio Valdés-Hernández[2] ·Jorge Bosch-Bayard[3] · Naoya Oosugi[4] · Misako Komatsu[5] · Naotaka Fujii[4] · Pedro Antonio Valdés-Sosa[1, 6, *]

1. The Clinical Hospital of Chengdu Brain Science Institute, MOE Key Lab for Neuroinformation, University of Electronic Science and Technology of China, Chengdu, China;
2. Department of Biomedical Engineering, Florida International University, Miami, FL, United States;
3. Unity of Neurodevelopment, Institute of Neurobiology, UNAM, Campus Juriquilla, Santiago de Querétaro, Querétaro, México;
4. Laboratory for Adaptive Intelligence, RIKEN Brain Science Institute, Saitama, Japan;
5. Laboratory for Molecular Analysis of Higher Brain Function, RIKEN Center for Brain Science, Saitama, Japan;
6. Cuba Neuro Science Center, La Habana, Cuba.

Abstract

Concurrent electroencephalography (EEG) and electrocorticography (ECoG) recordings (namely EECoG) constitutes a thorough gold standard to validating EEG generative models and developing EEG source imaging (ESI) methods. Primate models have the unique advantages of both flexibility and translational value in human research. However, the complexity of providing sufficiently detailed biophysical models as well as the typical severe EEG artifacts during such invasive experimental have hampered the availability of such datasets. In this paper, 1) we provide EECoG-Comp: an open source platform (https://github.com/Vincent-wq/EECoG-Comp) which encompasses the forward modeling and preprocessing modules; 2) we take the simultaneous EECoG dataset from the Multidimensional Recording (MDR) initiative (www.neurotycho.org) launched by Dr. Naotaka Fujii's group as an example, and share the realistic MRI-based head model (including the silicone stripes scaffolding the intracranial ECoG electrodes), the corresponding EEG and ECoG realistic Finite Element Method (FEM) lead fields, and the cleaned EECoG dataset, respectively. As a demonstration of the possibilities that EECoG-Comp brings, we preliminarily show how resting state connectivity between EEG electrodes misleadingly proxies the more plausible pattern of cortical functional connectivity calculated directly from ESI solutions. EECoG-Comp has been already used in several publications we foresee as the pillars of a more systematic effort to 1) understanding how the cortical electrical activity is actually reflected in non-invasive electrophysiological scalp recordings—distant and filtered by volume conduction effects, 2) fine-tuning novel ESI methods. Given its highly translational value, EECoG-Comp furnishes the path to unravel human brain function and pathology.

Key words

EEG, ECoG, Lead Field, Artifact Suppression, Open Science

1 Introduction

Among the non-invasive technologies used to uncovering normal and pathological brain function and mental states in both humans and animals, Electroencephalography (EEG) (Schomer and Da Silva, 2012) is the most affordable, popular and widespread. It also scores among those with the highest

1 Qing Wang and Pedro Antonio Valdés-Hernández contributed equally to this paper.

temporal resolution. Alas, like any imaging modality, EEG is not a straightforward and invertible proxy to brain activity. It is a down-projected and filtered transformation of hidden brain states, corrupted by noise and artifacts.

Any hypothesis or conclusion drawn from EEG measurements must be considered with caution. At the EEG electrodes the signal is spatially filtered by volume conduction (van den Broek et al., 1998)—owing to the very low conductivity of the skull—mixing the contribution of the sources of the EEG. This convolution results in blurred scalp topographies that conceal the actual location of the EEG sources in the brain. It also introduces spurious values of brain coherence, leading to false brain connectivity estimations.

For this reason, EEG connectivity must be assessed directly from the sources, mandating the solution of the inverse problem (Pascual-Marqui, 1999) of EEG: the estimation of brain sources from EEG measurements—a technique usually called EEG Source Imaging (ESI). It requires the solution of the forward problem (Hallez et al. 2007) of the EEG first, i.e., the calculation of the so-called lead field matrix (LF)—a map from known sources to EEG measurements—which demands the definition of a head model specifying the spatial distribution of the tissue conductivity, the source space model and the localization of the position of the EEG electrodes relative to the latter. The more realistic the head model, the more accurate of the ESI solutions. Nowadays, high detailed anatomical Magnetic Resonance Images (MRI) are used to define the head model and either Boundary Element Methods (BEM) or Finite Element Methods (FEM) are used to calculate the LF.

On the other hand, the EEG inverse problem is ill-posed in the Hadamard sense: the null space of the lead field has finite dimension, sabotaging the uniqueness of the solution. Thus, it is necessary to impose priors on the sources like sparsity, smoothness or independence; and to restrict the source space with anatomical information, e.g. restricting the source space to gray matter and the orientation of the dipoles perpendicular to the cortical layer. This is another reason to provide accurate head models. Abundant inverse solutions have been developed and implemented like weighted minimum-norm estimation (WMNE) (Hämäläinen et al. 1994), beamforming (BF) (Grech et al. 2008), Blind Source Separation (BSS) (Oosugi et al. 2017), exact Low Resolution Electromagnetic Tomography (eLORETA) (Pascual-Marqui 2007), BC-VARETA (Gonzalez-Moreira et al. 2018), among others.

The accuracy of the EEG forward and inverse solutions is paramount to unveil brain function. However, to date, there is a paucity of ground truth to evaluate their accuracy on real EEG data—unsurprisingly, given the obvious difficulty in having scalp EEG signals in a normal, intact head simultaneously with direct brain activity measurements. This was only tackled with few unrealistic though exceptionally useful attempts in the past. That is the case of Leahy et al. (1998) who designed and conducted a multiple dipole phantom consisting of 32 independently programmable and isolated dipoles inserted in a skull mount filled with conductive gelatin. They used this phantom to collect EEG and MEG data to evaluate the performance of current dipole localization methods. In Marin et al. (1998) another realistic conductive skull phantom was used to evaluate the accuracy of forward FEM methods. Later, this phantom was used to evaluate the performance of different ESI methods in Baillet et al. (2001)[2]. None of the “simulated” sources placed in these phantoms reflected actual ongoing or evoked brain activity.

A much more useful “phantom” to study the effect of the accuracy of ESI on assessing brain connectivity and source localization is the one providing scalp EEG signals concurrently with actual and direct whole brain measures of brain activity. This rules out Local Field Potential (LFP) and Multi-Unit Activity (MUA) (Mattia et al. 2010), which are local, and optical imaging (Wang et al. 2003), which requires the removal of the skull during the experiment. A better candidate is the Electrocorticogram (ECoG), which is measured directly over the cortex and can be obtained simultaneously with scalp EEG after closing the skull. However, its invasiveness makes it available only in clinical and preclinical settings, mainly restricted to pathologies like epilepsy—only targeting the seizure onset zones and thus usually precluding the recording of larger spatial extensions of the cortex (Frauscher, et al. 2018). In turn, the same situation is much more advantageous in primates, the reason we steer to the Multidimensional Recording (MDR) database (http://neurotycho.org) (Nagasaka et al. 2011). This initiative provides the desired combination for the evaluation of the performance of different ESI methods in assessing brain connectivity in different mental states. Among other behavioral and biological data, it shares simultaneous EEG/ECoG recordings under closed eyes resting state and anesthesia of a Japanese macaque (*macaca fuscata*). Importantly, after the ECoG stripes are placed on the cortex, the skull and skin are placed back to cover the brain, providing an almost normal scalp EEG recording situation.

---

[2] Noteworthily, more recent and realistic phantoms, even 3D printed, are now available for these tests (Collier et al., 2012; Li et. Al 2013; Zhang et al. 2013).

Hitherto, there is no neuroinformatics platform (or pipeline) designed for ESI evaluations in this dataset. The main reasons are 1) the difficulty in obtaining a realistic head model that includes the very low conductivity of the ECoG silicone stripes that are inserted in below the skull; b) the artifacts induced by this very complicated experimental configuration, which hampers the correct estimation of brain sources and connectivity patterns. In this paper, we solve these problems and publicly provide put an open source platform named “EECoG-Comp”, based on MATLAB and FieldTrip (Oostenveld et al. 2011) data formats, alongside a clean, high quality, and ready-to-analysis version of the simultaneous EEG/ECoG version of data based on the MDR EECoG dataset. EECoG-Comp has the following features: 1) the realistic MRI-based biophysical head model, with a FEM-based LF matrix, accounting for the very low conductivity implanted ECoG stripes; 2) The customized preprocessing algorithms, including synchronization, and model-based artifact removal algorithms. We have shared this platform and the use example via (https://github.com/Vincent-wq/EECoG-Comp) (for the shared contents, refer to Tab. 1). The preliminary ESI results show the significant differences of “brain connectivity (covariance)” estimated with or without solving inverse problem. In fact, our platform and results have been used in the research of estimating directed connectivity (Papadopoulou et al. 2015) and testing the resolution properties of different inverse solutions (Todaro et al. 2018).

Tab. 1 Table of shared simultaneous EEG/ECoG data files.

Folders	Files	Description
1-Nii Images	mcSu_t1[bias corrected]-eq.nii	T1 MRI of the specimen (NIFTI file).
	Svbrain_cSu_t1[bias_corrected].nii	Brain mask.
	Masked_mcSu_t1[bias_corrected]-eq.nii	MRI with non-brain tissue masked out.
2-BrainSuite Segmentations	Csf_Su.nii	Binary cerebrospinal fluid mask.
	Gray_Su.nii	Binary gray matter mask.
	White_Su.nii	Binary white matter mask.
3-SPM Results	c1masked_mcSu_t1[bias corrected]-eq.nii	Probabilistic gray matter mask.
	c2masked_mcSu_t1[bias corrected]-eq.nii	Probabilistic white matter mask.
	c3masked_mcSu_t1[bias corrected]-eq.nii	Probabilistic cerebrospinal fluid mask.
	Masked_mcSu_t1[bias corrected]-eq_seg_inv_sn.mat	Inverse Transformation Template to individual.
	Masked_mcSu_t1[bias corrected]-eq_seg_sn.mat	Transformation from Template to individual.
4-Head Model	EcoG-elecs_Su-silicone_sheet.mat	Surface representing the set of silicone stripes.
	Hybrid3.nii	Image labeling the three head compartments.
	Inskull_Su-corrected.mat	Inner surface of the skull.
	Outskull_Su-corrected.mat	Outer surface of the skull.
	Scalp_Su.mat	Surface of the scalp (MATLAB patch format).
	EcoG-elecs_Su-embbed.mat	ECoG electrodes in the set of silicone stripes.
	EEG-elecs_Su.mat	EEG electrodes on the scalp.
	MESHmodel.2.ele	Elements of the FEM model (generated using TetGen).
	MESHmodel.2.face	Modes of the FEM model (generated using TetGen).
	Cortex-mid_Su.mat	Surface representing cortex.
5-Lead Fields	EcoG-leadfield.mat	Lead field for the EcoG data (MATLAB matrix).
	EEG-leadfield.mat	Lead field for the EEG data.
6-Atlas and Template	c1masked_macaque_25_model-MNI-eq.nii	Gray matter prior for the template.
	c2masked_macaque_25_model-MNI-eq.nii	White matter prior for the template.
	c3masked_macaque_25_model-MNI-eq.nii	Cerebrospinal fluid prior for the template.
	Macaque_25_model-MNI-eq.nii	Template MRI of Macaca Mulatta.
7-Pipelines	Forward_model_Su.zip	The forward modeling pipeline of the macaque head.
	Preproc_TARA_Su.zip	The preprocess pipeline of the macaque recordings.

2 Material and Methods

2.1 MDR Recording

This dataset is partly described in Nagasaka et al. (2011) and Oosugi et al. (2017). All the experimental and surgical procedures were performed in accordance with protocols approved by

RIKEN ethical committee (No. H22-2-202(4)) and the recommendations of the Weatherall report, “the use of non-human primates in research”. During the experiment, a macaque monkey (*macaca fuscata*) was seated in a primate chair with hands tied and head movement restricted. The eyes of the monkey were covered to avoid evoked visual responses during the entire experimental period.
The electrophysiological data (ECoG and EEG) was recorded during two conditions: 1) awake resting state and 2) drug induced anesthesia: 1.15 ml (8.8 mg/Kg) ketamine hydrochloride and 0.35 ml (0.05 mg/Kg) medetomidine injection. For each condition, two five-minute trials of simultaneous resting state EEG and ECoG activities were recorded.

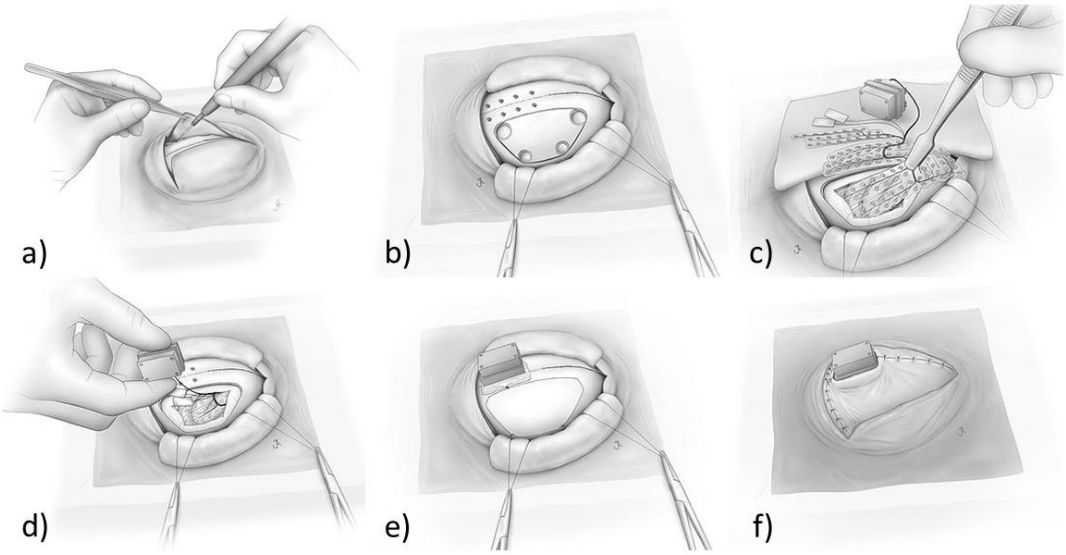

Fig. 1 The The surgery of implanting ECoG arrays.

For ECoG, the skin, skull and dura of the left hemisphere of the monkey was carefully removed. Then, a modified human subdural ECoG array, adapted to a monkey physiology (Nagasaka et. al., 2011), was inserted in the subdural space between the arachnoid membrane and the dura mater (see Fig. 1). This array consisted in a set of 1 mm-thick silicone stripes containing and insulating 128 ECoG platinum disk-shaped electrodes 3 mm in diameter, leaving only a hole in the silicone of 0.8 mm diameter at the center of each electrode. The electrodes, with a separation of 5 mm between each other, covered the frontal, parietal, temporal and occipital lobes and part of the medial wall of the left cortex, as depicted in the X-ray image in Fig. 2

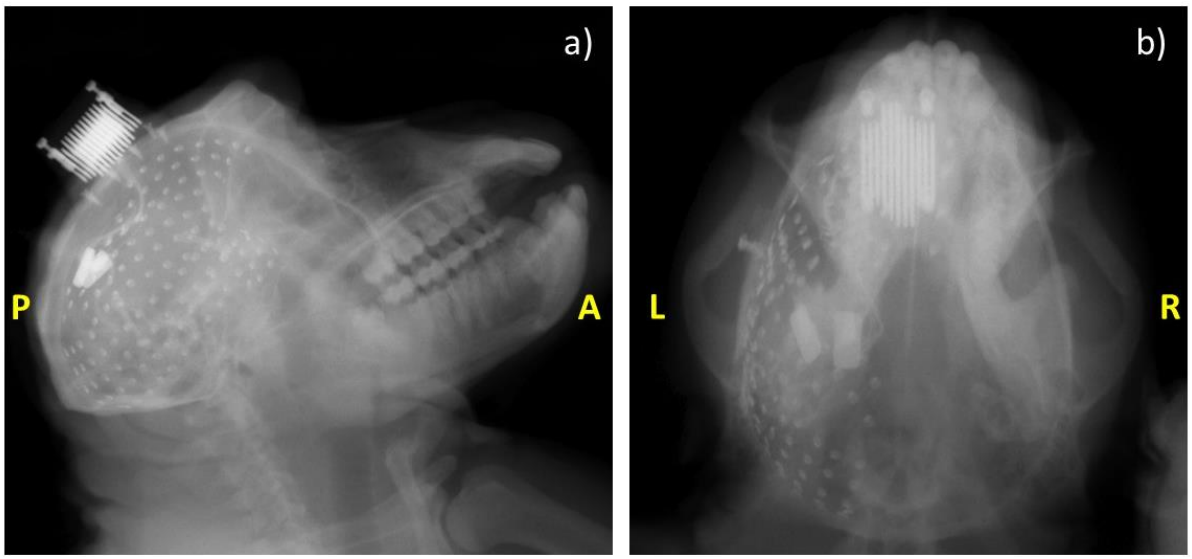

. The X-ray images were obtained by using the VPX-30E system (Toshiba Medical Supply, Tokyo, Japan) with 8.0 mA in current and 90 kV in voltage. The reference electrode were rectangular platinum plates in the subdural space between the array and the dura. Another platinum electrode

was placed as ground in the epidural space. After placing the ECoG electrodes, the dura, skull and skin were carefully placed back. ECoG was filtered and recorded by a Cerebus recording system (Blackrock Microsystems, Utah, USA). Plastic connectors from the array to the ECoG system were attached to the top of the head with dental cement and small titanium screws. The sampling rate was 1000 Hz, and the recordings were Butterworth bandpass filtered within 0.3-500 Hz.
On the other hand, EEG was recorded utilizing a NeuroPRAX system (eldith GmbH, Ilmenau, Germany), with sampling rate of 4096 Hz, using 18 electrodes following the standard 19-electrode 10-20 system, but removing electrode "Cz" to place the ECoG plastic connector. Data was down-sampled 1000 Hz. We share the data for both sampling rates. EEG and ECoG were triggered at the beginning and the end of each trial for synchronization using an external TTL pulse.

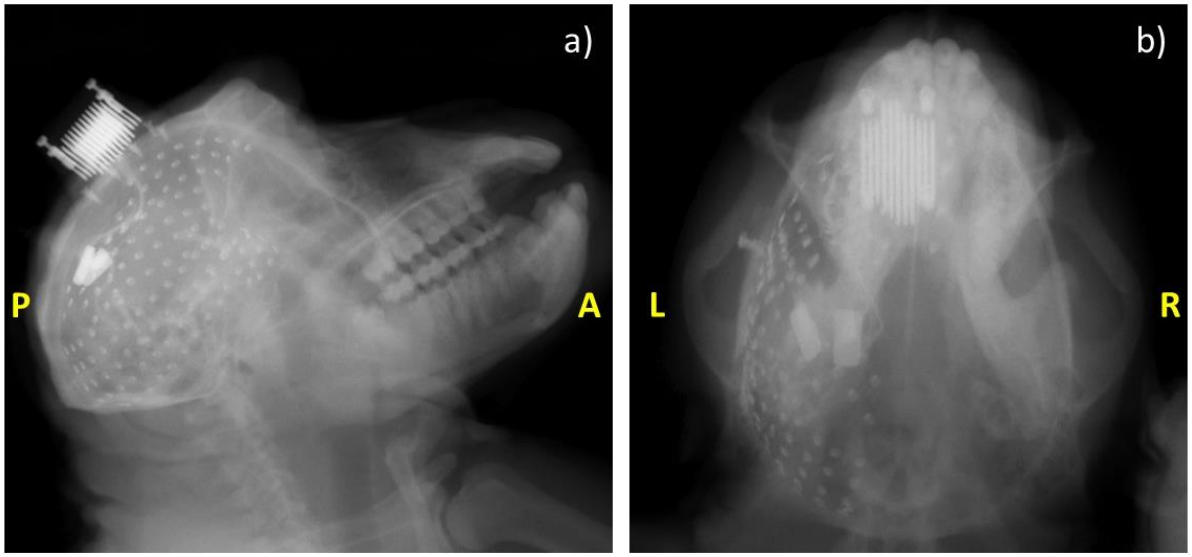

Fig. 2 X-ray images of the ECoG electrodes: 1) sagital view; b) coronal view.

2.2 Concurrent EEG/ECoG Comparison Open Source Platform

In this section, we introduce **EECoG-Comp**, the concurrent EEG/ECoG comparison open source platform, and break it down into its two main modules: **Forward Modeling** and **Preprocessing**. These, and their submodules, are shown in the diagram of Fig. 3. Both main modules aim to solve the above-mentioned problems present in simultaneous EEG/ECoG monkey data, respectively: 1) the difficulty in solving the EEG forward problem in the presence of the very thin silicone ECoG subdural array, and 2) the artifacts induced by the very complicated experimental configuration.

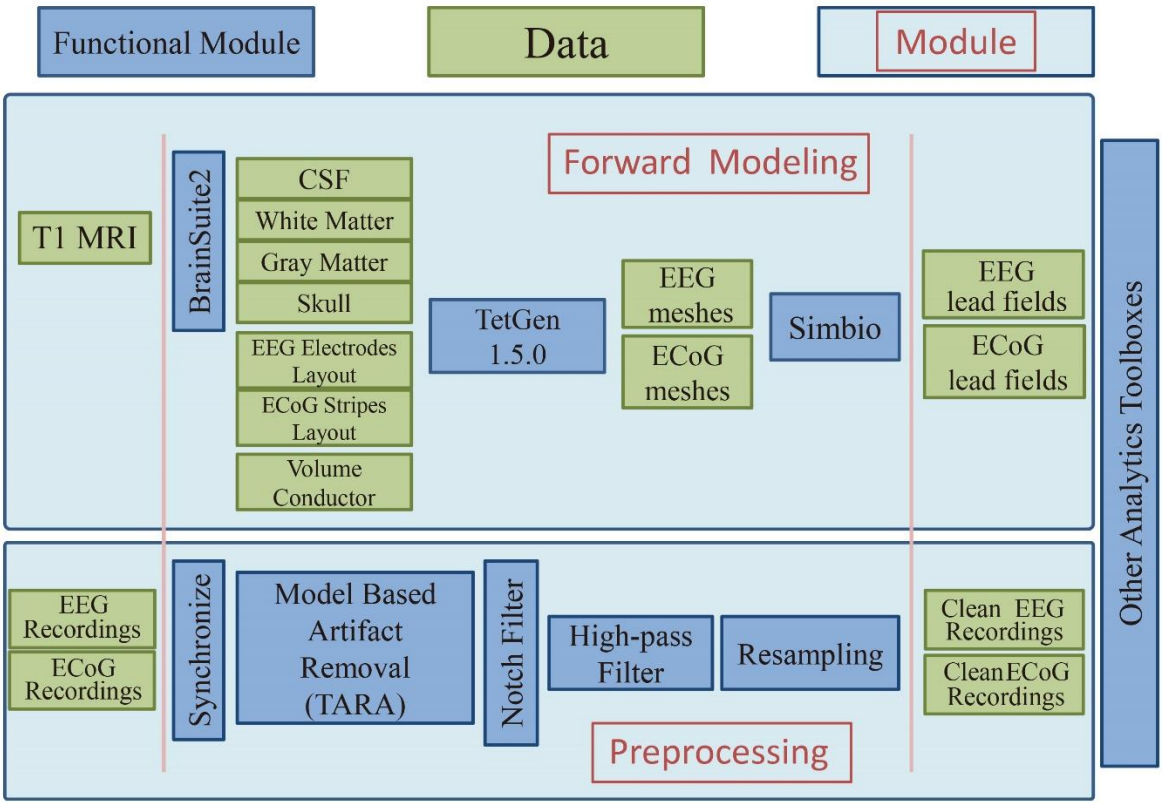

Fig. 3 Detailed system diagram for the open source EECoG-Comp with its main modules and submodules.

2.2.1 Forward Modeling: Head Modeling and Lead Field Calculation

The surfaces (triangular meshes) defining the head model were extracted from a T1-weigthed Magnetic Resonance Image of the monkey. This was acquired in a 4T Varian Unity Inova MR scanner (Varian NMR Instruments, Palo Alto, CA) with a 3 in single loop surface coil (Takashima Seisakusho Ltd.; Tokyo, Japan). The scanning parameters are: TR/TE = 13 ms/3.8 ms, in-plane matrix is $256 \times 256 \times 256$, field of view is $12.8 \times 12.8 \times 12.8\ cm$ with voxel size of $0.5 \times 0.5 \times 0.5\ mm$. This image was segmented into white matter (WM), gray matter (GM) and cerebrospinal fluid (CSF) with BrainSuite2 (Shattuck et al. 2001). The gray and white matter interface surface, shown in Fig 3a, was chosen as the source space model for EEG/ECoG, i.e. each of its 104650 nodes can be the location of a current dipole with orientation normal to the surface. The volume conductor model comprises three compartments 1) WM+GM+CSF, 2) Skull and, 3) Skin with constant conductivities 0.33 S/m, 0.0041 S/m and 0.33 S/m, respectively. These are represented by their boundaries, i.e. the “inskull”, the “outskull” and the “scalp”, which are shown in Fig. 3a. Additionally, a fourth compartment accounting for the ECoG silicone array was included, with 1 mm thickness and the shape shown in Fig. 1c, and also described in Section “MDR Recording”. It is very important to account for this compartment because its conductivity is very small (negligible as compared to the rest of the compartments) and therefore it is determinant on the EEG signals.

To locate the electrodes, the X-ray 2D image shown in Fig. 2, which was spatially registered to the projection of the pial surface to its leftmost sagittal slice. The transformed electrode positions were then projected onto the 3D pial surface. A schematic of these positions, imbedded in the silicone array, over the left cortex are represented in Fig. 4b. On the other hand, the EEG electrodes were manually located on the monkey’s scalp using IMAGIC (www.neuronicsa.com), as depicted in Fig. 4c.

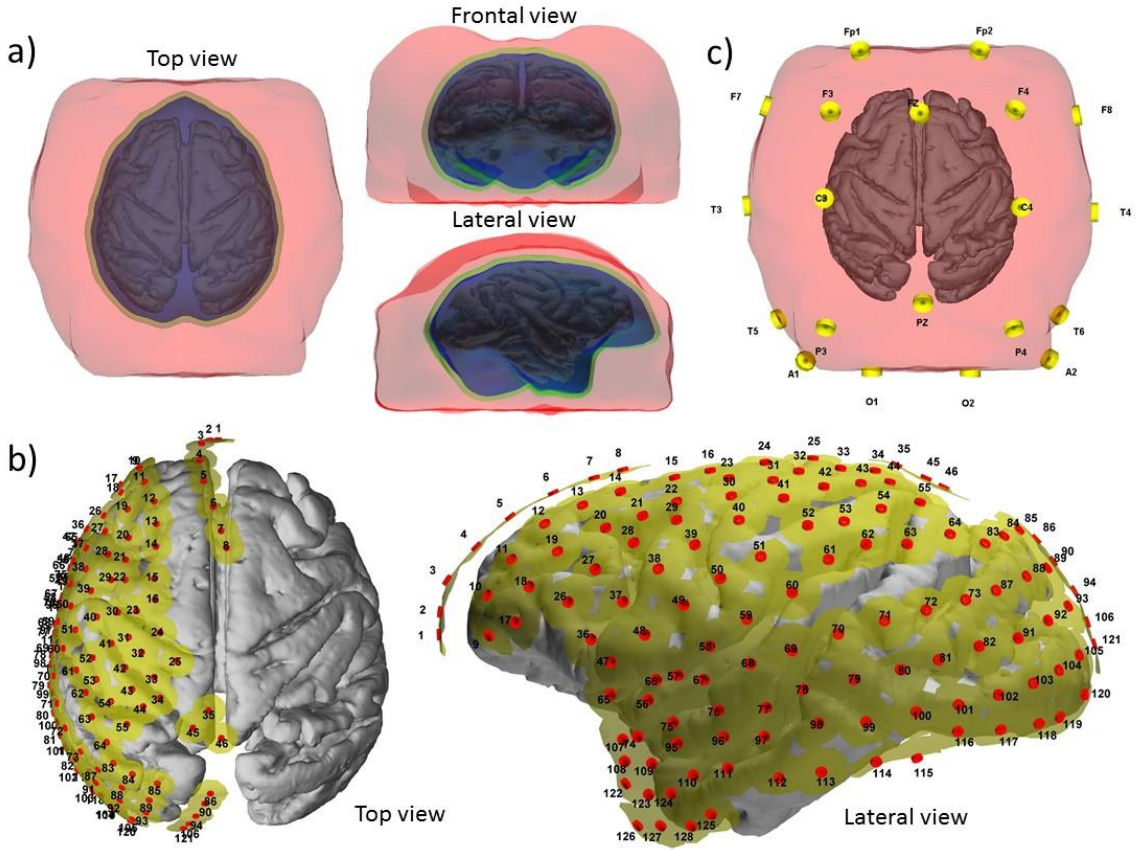

Fig. 4 Head Modeling of the monkey: a) surfaces defining the source space and the volume conductor model. From inside to outside: source space, inskull, outskull and scalp; b) silicone compartment (yellow) and 128 ECoG electrode positions represented—source space is shown as reference.

Tetrahedral meshes, shown in Fig. 5, were created from the surfaces of the head model using TetGen 1.5.0 (Si 2015), an open source software in Linux repositories. During the meshing process the nodes in the source space surface were forced to be nodes of the tetrahedral mesh to guarantee the Venant condition. Both EEG and ECoG lead fields were calculated using NeuroFEM. This is a program for computing lead fields using FEM which is part of the SimBio software package (Consortium et al. 2000) (index page: https://www.mrt.uni-jena.de/simbio /index.php/Main_Page). We provide average referenced LFs.

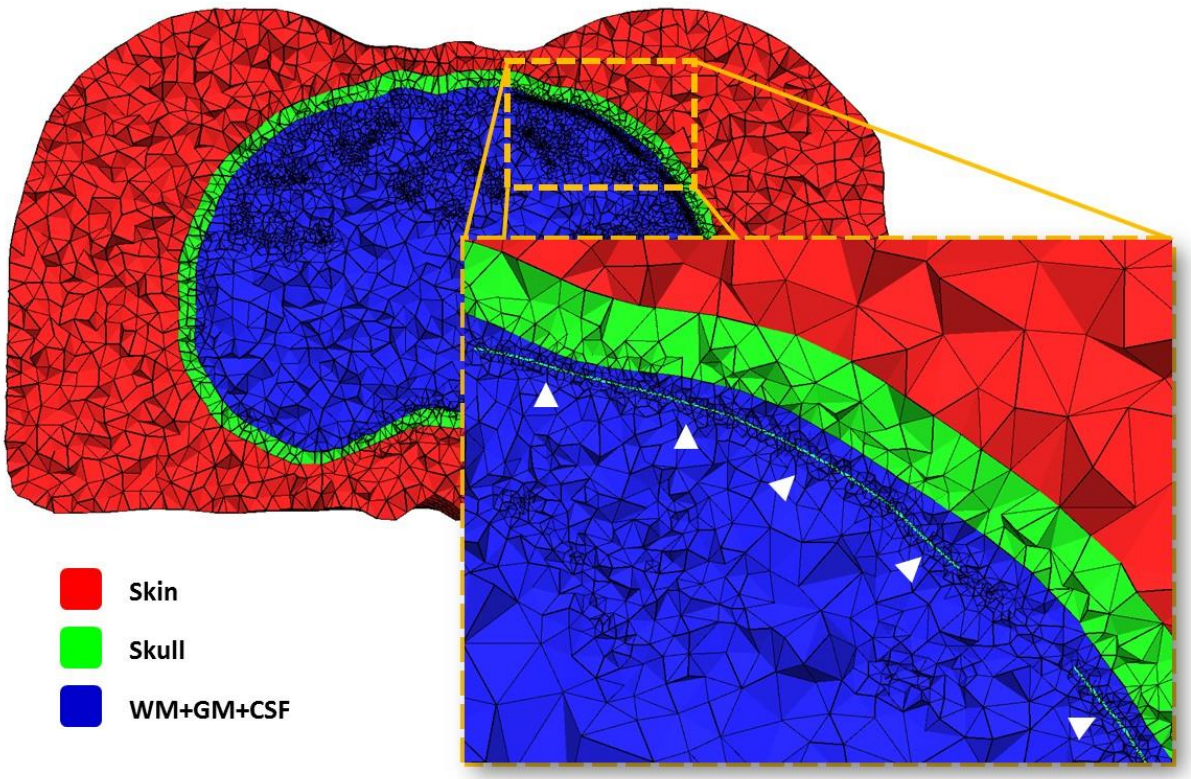

Fig. 5 Coronal slice of the tetrahedral mesh of the four compartments of the head model. The inset shows a zoom around the 1mm-thick silicone compartment, highlighted by the white arrows.

2.2.2 Preprocessing

In order to make the data easier to use, we format the original data into the FieldTrip (Oostenveld et al. 2011) data structure and do the following preprocessing in MATLAB. Basically, we started from the original 4096 Hz EEG recordings and 1000 Hz ECoG recordings, and then synchronize the two recordings by the “Trigger” signal, after that, we remove the “Trigger” channel for both EEG and ECoG recordings. After that, we apply the average reference. Based on the artifact properties of slow trend and sparse spikes of the EEG data, we further use the optimization-based algorithms TARA (Transient Artifact Reduction Algorithm) (Selesnick et al. 2014) to clean these artifacts (will be detailed in the Sect. 2.2.3). After the above procedures, we use the notch filter to remove the power-line artifact of 50 Hz and apply the Butterworth high-pass filter of 0.3 Hz. At last, we down-sampled the EEG recordings to 1000 Hz to match the sampling rate of ECoG recordings for better comparison. Till now the clean data is ready for further analysis.

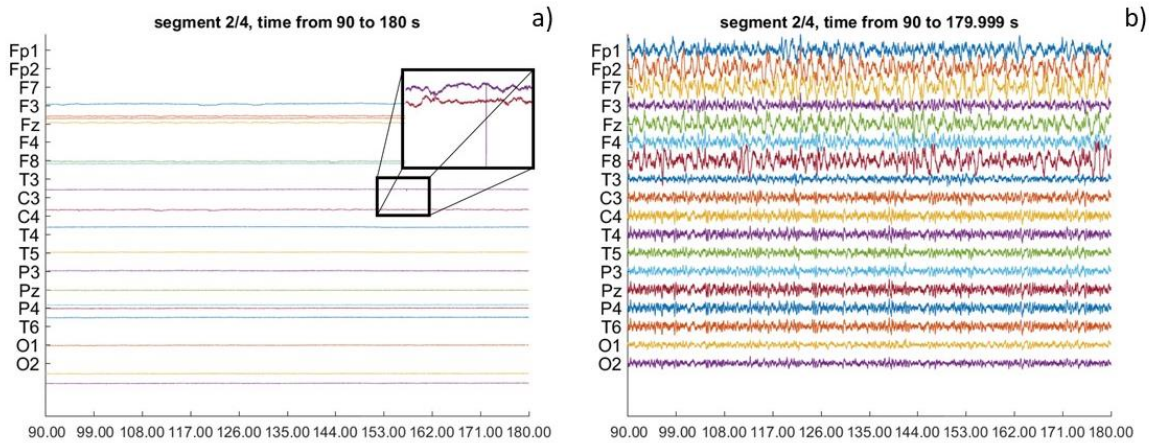

Fig. 6 The comparison of the EEG recordings before and after preprocessing. (a) The original EEG recordings of anesthesia trial 5 (Y scale is [-2909.6196, 2690.389]), the zoomed in window shows the artifacts of drifting and spikes in the original recordings. (b) The cleaned EEG recordings of anesthesia trial 5 (Y scale is [-60, 60]).

2.2.3 Model Based Artifact Removal

As illustrated in Fig. 6, the raw EEG data mainly suffered from 2 types of artifacts: Low frequency drifting and sparse spikes. In this paper, we introduce TARA and formulate the artifact removal problem in discrete-time setting, and the model (for one channel) can be written as:

$$y = x + a_1 + a_2 + \mu, (x, y, a_1, a_2 \in \mathbb{R}^N), \qquad \text{Equation 1}$$

among them, y is the recorded signal, while x is the low-pass discrete-time signal we aim to obtain, a_1 is the type1 artifact, which is the spare spike artifacts (spare of the signal itself and the first derivative), and a_2 is the type2 artifact, which is the slow drifting of the recorded signal (spare in its first derivative), μ is the additive gaussian noise. D is the first order difference operator. In our case, a_1, D_{a_1}, and D_{a_2} are modeled sparse. Based on this, the artifact removal procedure can be turned into an optimization problem:

$$\{\hat{a}_1, \hat{a}_2\} = arg \min_{a_1, a_2} \left\{ \frac{1}{2} \|H(y - a_1 - a_2)\|_2^2 + \lambda_0 \sum_n \phi_0([a_1]_n) + \lambda_1 \sum_n \phi_1([Da_1]_n) + \lambda_2 \sum_n \phi_2([a_2]_n) \right\}, \qquad \text{Equation 2}$$

where λ_i is regularization parameter, and ϕ_i is the penalty function promoting sparsity. H denotes the high-pass filter annihilating the low-pass signal x. The low-pass signal can then be estimated as:

$$\hat{x} = L(y - \hat{a}_1 - \hat{a}_2) = y - \hat{a}_1 - \hat{a}_2 - H(y - a_1 - a_2), \qquad \text{Equation 3}$$

where L is defined as the low-pass filter: $L = I - H$. By introducing TARA, we have successfully cleaned the above two types of artifacts, and original data and the clean data are compared in Fig. 6.

3 Preliminary Analysis

In this section, we demonstrate the effectiveness of EECoG-Comp by providing the simple spectrogram as well as the connectivity analysis at sensor and source level. Then we give the recommendations for using and sharing this platform and the example head model together with the cleaned data.

3.1 Sensor and Source Level Spectra

Spectrogram (squared magnitude of the Short-Time Fourier Transform (STFT)) is useful in analyzing neurological signals, but with drawback of leakage effect. To overcome this, we use the multi-tapper method and the implementation in Chronux (Bokil et al. 2010) and we find that the spectrogram is stable and consistent during the experiment. In order to compare

the spectrum of the EEG recordings, the ECoG recordings, the reconstructed EEG sources, and the reconstructed ECoG sources, we simply take the left occipital lobe as an example, for EEG, it is the O1 channel, for the ECoG it is channel 121, and the closest source (using eLORETA) is number 1634. The results are illustrated below in Fig. 7, it is clear that the source spectrum is different from the sensor spectrum for both EEG and ECoG, and it shows slower oscillations in anesthesia state than the awake state (<10 Hz), and more β oscillation (13-20 Hz) in the awake state, which is consistent with the previous experience. The estimated source spectrum from both EEG and ECoG in awake state looks similar, however, the sensor level spectrum differs a lot for EEG and ECoG. In the anesthesia state, all the spectrum looks similar.

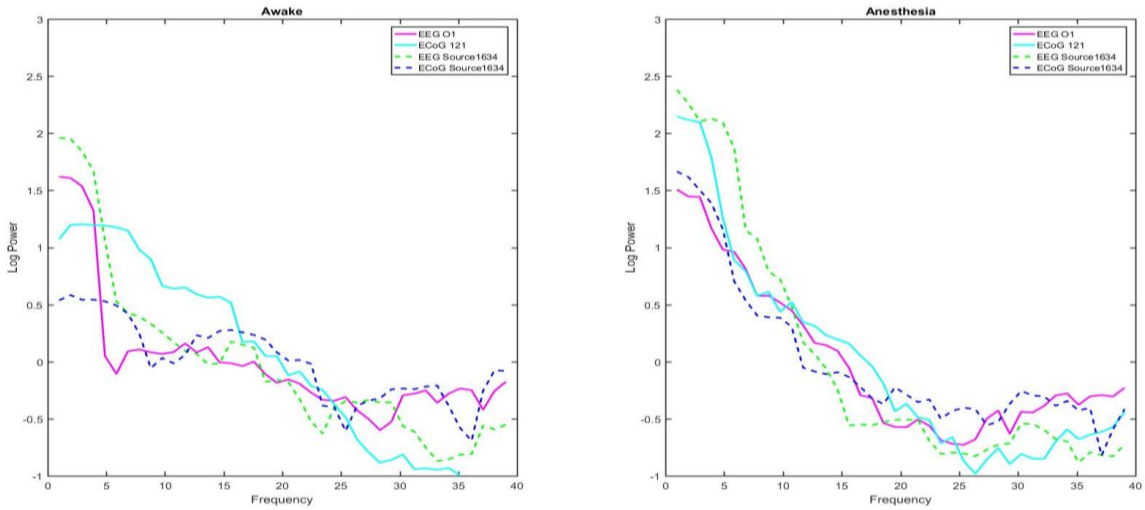

Fig. 7 The spectrum for the EEG/ECoG at sensor and source level for the left occipital lobe in awake (a) and anesthesia (b) state. (The y axis is the z-score in logarithm of the power in each frequency point. The solid lines are calculated from the cleaned recordings directly and the dashed lines are the reconstructed source spectrum.)

3.2 Sensor and Source Level Connectivity

Correlation or covariance is the most fundamental way to estimate the statistical dependence between two or multiple variables, and it has been applied widely in brain connectivity analysis like “functional connectivity” (Friston 2011). However, due to the unideal measurement of brain activities, it is difficult to estimate the brain connectivity. In this section, we use eLORETA (Pascual-Marqui et al. 2007)) and the lead field generated from EECoG-Comp to obtain the source activities and then compute the covariance matrix at the source level for both EEG and ECoG recordings. The results are visualized using BrainNetViewer (Xia et al. 2013) and illustrated in Fig. **8** for comparison, they are the sensor level connectivity for EEG (18 sensors and covariance threshold 0.8) in Fig. **8**a, the source level connectivity for EEG (4957 sources and covariance threshold 0.9999) in Fig. **8**b, the sensor level connectivity for ECoG (128 sensors and covariance threshold 0.8) in Fig. **8**c, the source level connectivity for ECoG (4957 sources and covariance threshold 0.998) in Fig. **8**d.

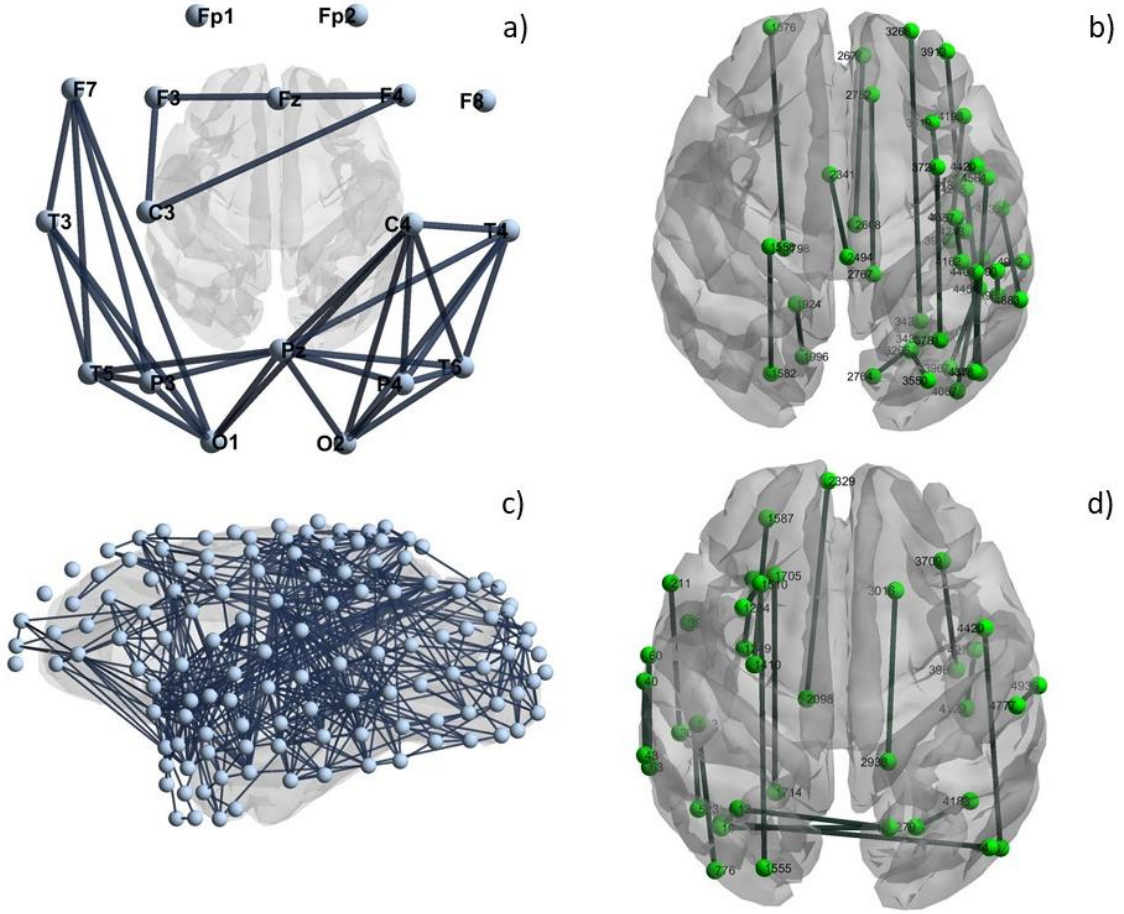

Fig. 8 Preliminary results of the EEG/ECoG connectivity comparison in sensor and source level: a) EEG sensor level connectivity; b) EEG source level connectivity; c) ECoG sensor level connectivity; d) ECoG source level connectivity.

By comparing the 4 figures, we can see that: 1) The connectivity are not the same at sensor and source level no matter it is EEG or ECoG; 2) Even using the same inverse method (eLORETA) and configuration, the source level connectivity for EEG and ECoG is totally different, EEG shows denser connectivity due to much severer volume conduction (The visualization tools only support limited number of connections for each rendering, thus we choose higher threshold for EEG, even though, the number of EEG source connections left is larger); 3) The source connectivity estimated from EEG are located mainly on the right hemisphere, whereas the source connectivity estimated from ECoG is mainly on the left hemisphere. This can be the result of implanting the ECoG stripes, which improves the spacial resolution of ECoG source connectivity on the left hemisphere while affecting the simultaneous EEG recordings, thus decreasing the EEG source connectivity on the left hemisphere. The results are interesting and important for connectivity estimation. The aim of this section is to show the application and results of EECoG-Comp, and further comprehensive analysis is beyond the scope of this paper.

4 Discussion

In this paper, we provide EECoG-Comp, an open source EEG and ECoG comparison platform, which provides the realistic biophysical forward models for EEG and ECoG comparison and TARA based artifact removal algorithm.

The preliminary results are interesting, we can see clear differences among both spectrum and connectivity (coherence) calculated from the EEG signal, the ECoG signal, the reconstructed EEG source signal, and the reconstructed ECoG source signal. We also notice that the implanting of ECoG stripes affected the connectivity among sources, which should be taken into consideration when comparing different ESI methods.

5 Conclusion

In this paper, we first provide the open source EECoG-Comp platform, which aims to build the realistic biophysical forward model for the EEG and ECoG comparison problem, it has great potential in solving the following problems: 1) evaluate the effectiveness of EEG (compare to ECoG); 2) evaluate different ESI methods; 3) evaluate different connectivity estimators. In order to demonstrate this platform, we take the simultaneous EEG/ECoG data of a (*macaca fuscata*) from neurotycho.org as an example, build the head model with FEM, clean the data and solve the inverse problem with eLORETA. As the preliminary results, we present the spectrum and connectivity estimates from the EEG signal, the ECoG signal, the reconstructed source signal from EEG, and the reconstructed source signal from ECoG, all of them are different. The results show the inconsistency of estimating brain activity and connectivity from sensor and source levels, which needs further research and comparison, where EECoG-Comp can serve as the basic platform to start with.

Acknowledgements and author contributions

The authors would like to thank the helpful discussions with Carsten Wolters, Marios Antonakakis, Maria Carla Piastra, and Laura Marzetti in forward modeling, and the discussion with Peng Ren and Deirel Paz-Linares in the preprocessing of the data. The authors also would like to thank for the support from the C-C-C (China-Cuba-Canada) project and fund from National Nature and Science Foundation of China (NSFC) with funding No. 61673090, and 81330032.

References

C. Todaro, L. Marzetti, P. A. Valdés-Sosa, P. A. Valdés-Hernandez, and V. Pizzella (2018) Mapping Brain Activity with Electrocorticography: Resolution Properties and Robustness of Inverse Solutions. Brain Topography, pages 1–16,

D. L. Schomer and F. L. Da Silva (2012) Niedermeyer's electroencephalography: basic principles, clinical applications, and related fields. Lippincott Williams & Wilkins

D. W. Shattuck, S. R. Sandor-Leahy, K. A. Schaper, D. A. Rottenberg, and R. M (2001) Leahy. Magnetic resonance image tissue classification using a partial volume model. NeuroImage, 13(5):856–876

Eduardo Gonzalez-Moreira, Deirel Paz-Linares, Eduardo Martinez-Montes, Pedro Valdes-Hernandez, Jorge Bosch-Bayard, Maria Luisa Bringas-Vega, Pedro Valdes-Sosa (2018) bioRxiv 346569; doi: https://doi.org/10.1101/346569

Frauscher B, von Ellenrieder N, Zelmann R, et al. (2018) Atlas of the normal intracranial electroencephalogram: neurophysiological awake activity in different cortical areas. Brain, 141(4): 1130-1144

H. Bokil, P. Andrews, J. E. Kulkarni, S. Mehta, and P. P. Mitra (2010) Chronux: a platform for analyzing neural signals. Journal of Neuroscience Methods, 192(1):146–151

H. Hallez, B. Vanrumste, R. Grech, J. Muscat, W. De Clercq, A. Vergult, Y. D'Asseler, K. P. Camilleri, S. G. Fabri, S. Van Huffel, et al (2007) Review on solving the forward problem in EEG source analysis. Journal of Neuroengineering and Rehabilitation, 4(1):46

H. Si. (2015) TetGen, a Delaunay-based quality tetrahedral mesh generator. ACM Transactions on Mathematical Software (TOMS), 41(2):11

I. W. Selesnick, H. L. Graber, Y. Ding, T. Zhang, and R. L. Barbour (2014) Transient artifact reduction algorithm (TARA) based on sparse optimization. IEEE Transactions on Signal Processing, 62(24):6596–6611

K. J. Friston. (2011) Functional and effective connectivity: a review. Brain connectivity, 1(1):13–36

K. Mahjoory, V. V. Nikulin, L. Botrel, K. Linkenkaer-Hansen, M. M. Fato, and S. Haufe (2017) Consistency of EEG source localization and connectivity estimates. Neuroimage, 152:590–601

Leahy, R. M., Mosher J C, et al. (1998) A study of dipole localization accuracy for MEG and EEG using a human skull phantom. Electroencephalography and Clinical Neurophysiology 107.2: 159-173

Marin G, Guerin C, Baillet S, et al. (1998) Influence of skull anisotropy for the forward and inverse problem in EEG: simulation studies using FEM on realistic head models. Human Brain Mapping, 6(4): 250-269

Mattia M, Ferraina S, Del Giudice P. (2010) Dissociated multi-unit activity and local field potentials: a theory inspired analysis of a motor decision task. Neuroimage, 52(3): 812-823

M. Papadopoulou, K. Friston, and D. Marinazzo (2015) Estimating directed connectivity from cortical recordings and reconstructed sources. Brain Topography, https://doi.org/10.1007/s10548-015-0450-6

M. S. Hämäläinen and R. J. Ilmoniemi (1994) Interpreting magnetic fields of the brain: minimum norm estimates. Medical Biological Engineering Computing, 32(1):35–42

M. Xia, J. Wang, and Y. He. (2013) Brainnet viewer: a network visualization tool for human brain connectomics. PLoS ONE, 8(7): e68910

N. Oosugi, K. Kitajo, N. Hasegawa, Y. Nagasaka, K. Okanoya, and N. Fujii (2017) A new method for quantifying the performance of EEG blind source separation algorithms by referencing a simultaneously recorded ECoG signal. Neural Networks, 93:1–6

P. Xanthopoulos, V. Sakkalis, and B. Vanrumste (2008) Review on solving the inverse problem in EEG source analysis. Journal of Neuroengineering and Rehabilitation, 5(1):25

R. D. Pascual-Marqui (1999) Review of methods for solving the EEG inverse problem. International Journal of Bioelectromagnetism, 1(1):75–86

R. D. Pascual-Marqui. (2007) Discrete, 3d distributed, linear imaging methods of electric neuronal activity. part 1: exact, zero error localization. arXiv preprint arXiv:0710.3341

R. Grech, T. Cassar, et al. (2008) Review on solving the inverse problem in EEG source analysis. Journal of Neuroengineering and Rehabilitation, 5(1):25

R. Oostenveld, P. Fries, E. Maris, and J.-M. Schoffelen (2011) FieldTrip: open source software for advanced analysis of MEG, EEG, and invasive electrophysiological data. Computational Intelligence and Neuroscience, 2011:1

S. Consortium et al. (2000) Simbio: A generic environment for bio-numerical simulation

S. P. van den Broek, F. Reinders, M. Donderwinkel, and M. Peters (1998) Volume conduction effects in EEG and MEG. Electroencephalography and Clinical Neurophysiology, 106(6):522–534

Shattuck, D. W., & Leahy, R. M. (2002) BrainSuite: an automated cortical surface identification tool. Medical Image Analysis, 6(2):129-142

Wang X, Pang Y, Ku G, et al. (2003) Noninvasive laser-induced photoacoustic tomography for structural and functional in vivo imaging of the brain. Nature Biotechnology, 21(7): 803

Y. Nagasaka, K. Shimoda, and N. Fujii (2011) Multidimensional recording (MDR) and data sharing: an ecological open research and educational platform for neuroscience. PLoS ONE, 6(7):e22561